Laser-Induced Damage in Optical Materials

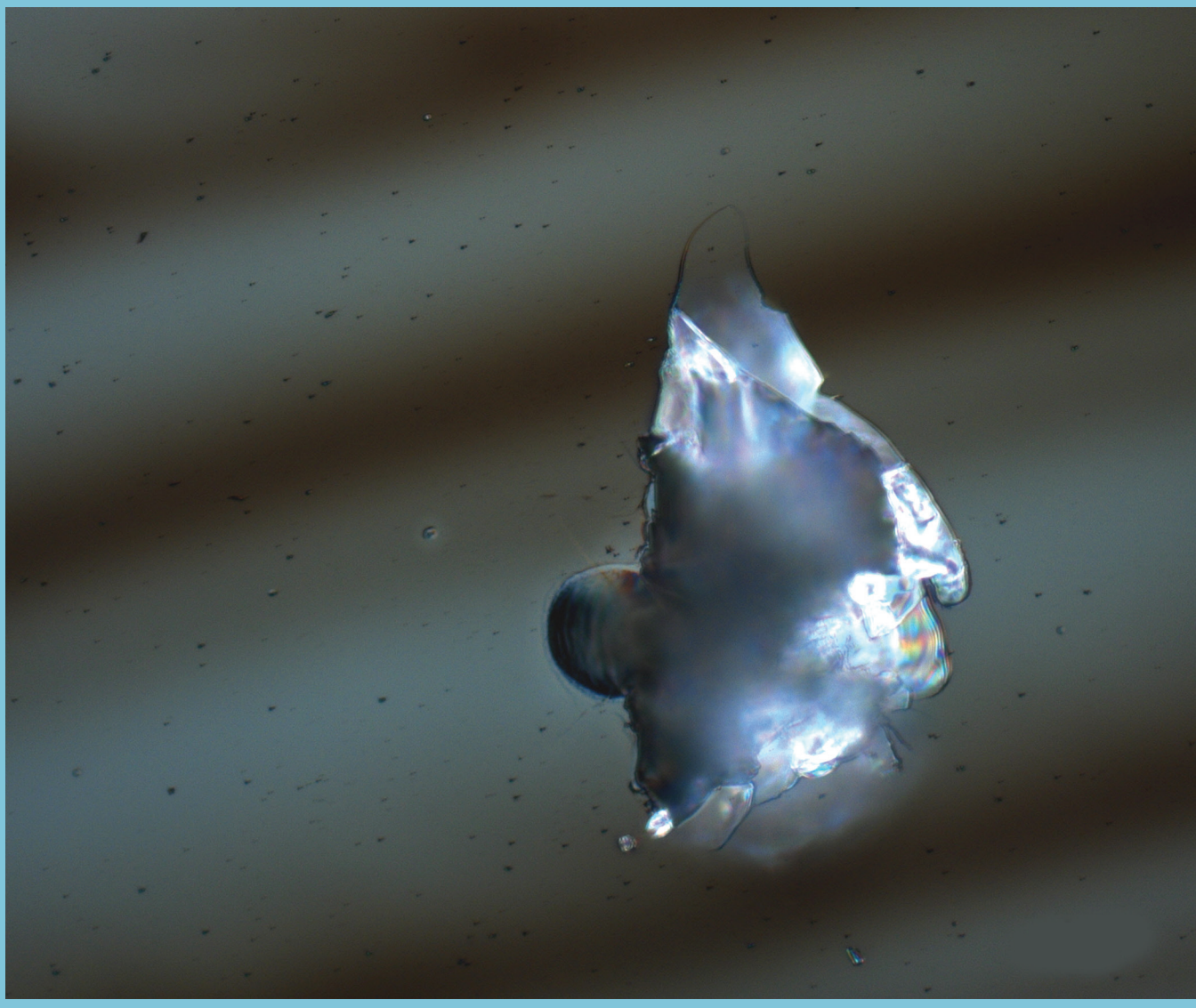

Edited by

Detlev Ristau

CRC Press
Taylor & Francis Group

Laser-Induced Damage in Optical Materials

Laser-Induced Damage in Optical Materials

Edited by
Detlev Ristau
Leibniz University of Hannover, Institute for Quantum Optics; and
Laser Zentrum Hannover, Department of Laser Components
Hannover, Germany

CRC Press
Taylor & Francis Group
Boca Raton London New York

CRC Press is an imprint of the
Taylor & Francis Group, an **informa** business

CRC Press
Taylor & Francis Group
6000 Broken Sound Parkway NW, Suite 300
Boca Raton, FL 33487-2742

Version Date: 20140929

International Standard Book Number-13: 978-1-4398-7217-8 (eBook - PDF)

To Dr. Arthur H. Guenther (1931–2007)
Founding Organizer of the Boulder Damage Symposium

Contents

SECTION III Materials, Surfaces, Thin Films, and Contamination

SECTION IV Applications

Preface

Since the very beginning of laser technology, the limitations in the power-handling capability of optical components were always an obstacle for the development of laser systems and applications operating at high power levels and improved beam quality. In the early days of laser development, mainly the inclusions in laser rod materials were discussed as a major complication in the augmentation of the output power in solid-state laser systems. Nowadays, in the course of the development of optical materials with excellent quality and power-handling capability, the problem of laser-induced damage has shifted from the bulk to the surface of the optical component. During the last two decades, considerable progress has been achieved by an ever-growing scientific community working in various areas of high-power optical materials and components. For example, the development of stable coatings for ultrashort pulse systems was an essential milestone in the introduction of femtosecond (fs) lasers, which in turn initiated novel and exciting research fields and industrial and even medical applications. These advances were complemented by significant progresses in the theoretical modeling of fs laser–induced damage phenomena resulting in a deeper understanding of the underlying electronic excitation effects. Semiconductor lithography, with its trend toward shorter wavelengths, is another essential pacemaker in the development of high-power optics with long lifetimes. Nowadays, industrial stepper systems operating at the wavelength 193 nm of the ArF excimer laser depend on optics with extremely high quality and stability. Also, the first tools of the next generation of lithography based on imaging procedures in the extreme ultraviolet (EUV) spectral region have been implemented with the target of reaching even smaller half-pitch values well below 20 nm for integrated circuit designs. Some of the wide variety of prominent applications in fundamental research where high-power lasers play an important role are laser medicine, gravitational wave detection, and nuclear fusion. Looking back more than 50 years since the demonstration of the first ruby laser, it is apparent that the history of laser technology cannot be written without mentioning the advances in optical high-power materials and components.

The subject of this book is the emerging area of research in laser damage occurring in the bulk and on the surface or the coating of optical components. Far from covering all aspects of laser damage published in thousands of scientific papers during the last five decades, the present compilation is intended to offer a comprehensive overview on recent developments in this vivid field. The main idea is to provide a fundamental reference for readers interested in the various fields of laser technology, photonics, or fundamental research, as well as optical component, material, and coating production.

Focusing on the major topics of laser-induced damage in optical materials, this book is divided into four sections. The first section is dedicated to the fundamentals of laser damage and is introduced by a brief history including major definitions and developments in the field. In the four chapters that follow, the dominating laser damage mechanisms are discussed, including thermal degradation effects, defect-induced damage, and select nonlinear effects leading to catastrophic failures of optical media. The final

chapter of the first section discusses the latest theoretical approaches in the description of damage phenomena in the ultrashort pulse regime.

The reliable measurement of laser-induced damage thresholds and related quality parameters of optical components is a major prerequisite for research in high-power optics and their optimization. In this context, the second section of the book gives an overview on the measurement and detection of laser damage as well as on the evaluation of statistical data recorded during the applied measurement protocols. The corresponding two chapters are of central importance for the understanding and ranking of laser damage data published in the literature and often also in the catalogs of optics suppliers. This section is rounded off by a comprehensive overview on the measurement of transfer properties and scatter losses of optics.

The third section of the book comprises detailed information on the involvement of materials, surfaces, and thin films in laser damage phenomena. In view of the enormous diversity of available scientific models and experimental results, a few current topics have been selected as examples representing the major branches of recent research as well as providing fundamental physics, relations, and data. The first three chapters are devoted to studies on materials for high-power lasers and concentrate on prominent applications mainly in the ultraviolet (UV), visible (VIS), and near-infrared (NIR) spectral regions. In this context, quartz and glasses are the most important material class and are considered within an extended chapter. The second chapter in the sequence discusses crystalline materials, especially for the UV spectral region and gives a comprehensive insight into related optical quality factors. Also of highest significance are optical materials for modern laser systems including active laser materials, frequency conversion crystals, and Q-switching materials, which are addressed in the third chapter of Section III. Following the production chain for optical components, the next step is the realization of an adequate surface quality, aspects of which are summarized in the fourth chapter of this section. After a general overview on optical coatings, which is the basis for all the following chapters of the book, two chapters on the optimization of coatings for NIR and fs lasers are included as examples illustrating the vast extent of research concentrated on high-power laser coatings. The final chapter of Section III compiles interesting aspects on the application of optical components for space-born laser systems and also addresses the contamination effects on optical surfaces under laser irradiation.

A book on laser-induced damage cannot be complete without a few insights into typical application areas of high-power coatings. In view of the huge impact of lithography on the development, a chapter on optics for deep ultraviolet (DUV) and EUV regions begins the last section, Section IV, which is on applications. Further applications considered exemplarily in the last two chapters are optics for free-electron lasers and for the large, high-power laser system PHELIX.

The authors of these chapters are associated with renowned research institutes and large-scale laser facilities active in the field for several decades. We hope that this complementary collection of scientific material, fundamental data, and practical information will be of general use and stimulate the interest of scientists, engineers, and technicians to gain deeper insights into the fascinating field of laser damage and its key role in laser technology.

Our thanks are due to the contributors, especially for their time and dedication in writing the chapters alongside their regular obligations and work schedules.

Editor

Detlev Ristau completed his study of physics at the University of Hannover in 1982 and was awarded a scholarship at Rice University in Houston, Texas, where he was working in the field of tunable color center lasers. He returned to Germany in 1983 and started his PhD research on the power-handling capability of optical coatings in the thin film group of the Institut für Quantenoptik at the University of Hannover. He earned a PhD in 1988 and was responsible for the thin film group at the institute until 1992. Professor Ristau is presently the director of the Department of Laser Components at the Laser Zentrum Hannover. After receiving a state doctorate in 2008, he was appointed professor for applied physics at the Leibniz University in Hannover in 2010, and he also assumed responsibility for a research group on ultrahigh-quality optical lasers.

Professor Ristau is the author or coauthor of more than 300 technical papers and has published several book chapters. His current research activities include the development and precise control of ion processes as well as the measurement of the power-handling capability and losses of optical components.

Contributors

Jonathan W. Arenberg
Northrop Grumman Space Technology
Vehicle Systems Engineering and Operations
Redondo Beach, California

Stefan Borneis
GSI Helmholtzzentrum für Schwerionenforschung GmbH
PHELIX/PP
Darmstadt, Germany

Philippe Cormont
Commissariat à L'Energie Atomique
Le Barp, France

Angela Duparré
Fraunhofer Institute for Applied Optics and Precision Engineering (IOF)
Jena, Germany

Luke A. Emmert
Department of Physics and Astronomy
University of New Mexico
Albuquerque, New Mexico

Vitaly Gruzdev
University of Missouri
Columbia, Missouri

Anne Hildenbrand-Dhollande
French-German Research Institute of Saint-Louis
Saint-Louis, France

Marco Jupé
Laser Zentrum Hannover
Department of Laser Components
Hannover, Germany

Laurent Lamaignère
Commissariat à L'Energie Atomique
Le Barp, France

H. Angus Macleod
Thin Film Center
Tucson, Arizona

Klaus R. Mann
Laser Laboratorium Göttingen
Göttingen, Germany

Christian Mühlig
Department of Microscopy—Laser Diagnostics
Leibniz-Institute of Photonic Technology (IPHT)
Jena, Germany

Jérôme Néauport
Commissariat à L'Energie Atomique
Le Barp, France

Semyon Papernov
Laboratory for Laser Energetics
University of Rochester
Rochester, New York

Wolfgang Riede
Deutsches Zentrum für Luft- und Raumfahrt e. V.
Institut für Technische Physik
Stuttgart, Germany

Detlev Ristau
Leibniz University of Hannover
Institute for Quantum Optics
and
Laser Zentrum Hannover
Department of Laser Components
Hannover, Germany

Wolfgang Rudolph
Department of Physics and Astronomy
University of New Mexico
Albuquerque, New Mexico

Sven Schröder
Fraunhofer Institute for Applied Optics
and Precision Engineering (IOF)
Jena, Germany

Jianda Shao
Shanghai Institute of Optics and Fine
Mechanics, CAS
Shanghai, People's Republic of China

Michelle Shinn
Accelerator Division Management
Department
Thomas Jefferson National
Accelerator Facility
Newport News, Virginia

M.J. Soileau
CREOL
The College of Optics and Photonics
University of Central Florida
Orlando, Florida

Christopher J. Stolz
Lawrence Livermore National
Laboratory
Livermore, California

Wolfgang Triebel
Department of Microscopy—Laser
Diagnostics
Leibniz-Institute of Photonic
Technology (IPHT)
Jena, Germany

Frank R. Wagner
Institut Fresnel
Aix-Marseille Université
Marseille, France

Denny Wernham
European Space Research
and Technology Center
Noordwijek, The Netherlands

Roger M. Wood (retired)
Cosolas Ltd.
Trimpley, Worcestershire,
United Kingdom

1 Fundamentals

1. Laser-Induced Damage Phenomena in Optics

A Historical Overview

M.J. Soileau

1.1 Introduction: The First Laser-Induced Damage

On May 21, 1960, Ted Maiman demonstrated the first laser [1]. The elegantly simple device consisted of a helium flash lamp designed for photography and a metal cylindrical sleeve to help direct the light from the lamp to a ruby rod, the laser gain medium. The laser resonator was simply the ruby rod with silver coatings on both ends, with one coating thin enough to allow particle transmission to couple out the energy generated and stored in the resonator.

Laser-induced damage (LID) quickly followed. Though the archival record is sparse on this topic, conversations with pioneers of the laser indicate common problems with the output coupling films [2,3]. It was common for laser researchers to keep "*spare*" ruby rods for use when the output coatings started to fall off.

These early lasers had pulse width related to the time width of the pump lamp, about 0.4 ms, and output energies of up to 5 J from 3 mm radius ruby rods, or about 10,000 W of power. The output of these early devices had multispatial and temporal modes. Particle mode locking of temporal modes and interference among the multiple modes likely resulted in peak powers on the order of hundreds of kilowatts.

The invention of the Q-switch quickly followed the invention of the laser discovered in 1961 and published in 1962 [3]. Q-switching reduced laser pulse width to the order of tens of nanoseconds from values of hundreds of microseconds in ruby and other solid state lasers. This resulted in factors of 10,000 or more increases in peak power. The so-called

Laser-Induced Damage in Optical Materials. Edited by Detlev Ristau © 2015 CRC Press/Taylor & Francis Group, LLC. ISBN: 978-1-4398-7216-1.

giant pulses easily damaged laser rods, cavity reflectors, Q-switch materials, and other optical components used to make the laser emitting the pulse. LID thus became a dominant feature in laser design and laser operations and remains half a century later. Partially transmitting metal film (sometimes called *soft coatings*) gave way to then called *hard* coatings made of transparent dielectrics and designs utilizing Brewster angle cut rods, external resonators, and, in some cases, reflectors and output couplers made of uncoated etalons. In addition, conventional material growth techniques had to be replaced to produce laser media with greatly reduced defects and impurities, all with the objective of reducing LID in the laser medium by the intense light produced within the medium.

Within 1 year after the invention of the ruby laser, McClung and Hellwarth reported difficulty of laser operation due to the fact that "output light burned holes in the silvered surfaces" on the ruby laser rod [3].

1.2 Development of High-Power Lasers

Precision optical components were rapidly developed in the World War II period, including multilayer, thin film coating to control reflection in complex optical systems. Quality control was essential for high resolution optics. Optical crystals and glasses needed to be free of strain to maintain resolution and avoid unwanted polarization effects. Smooth surfaces, without large amounts of scratches and digs, were produced to reduce scattering losses and increase image quality.

Thus, early laser builders had access to relatively high quality optics. However, while a surface defect may only marginally degrade an image, it can be the site of the initiation of catastrophic LID. Small amounts of absorption—say 1 part in 1000—do not diminish the functionality of an optical component in nonlaser applications but can easily result in damage to a surface, or delineation or ablation of a thin film. In fact, absorbing sites or defects sufficient to initiate catastrophic LID often escape detection using conventional techniques, for example, measurement of absorption by conventional spectrometers.

The demonstration of the first ruby laser served as a sort of *proof of existence* for lasers. An explosion of scientific and engineering efforts quickly followed as new laser sources were sought. This in turn drove the need for precision beam control and optical components needed for the many innovative ideas for laser applications that followed the laser's invention.

These new high-power optical devices became immediate tools to study nonlinear optics, and became victims of nonlinear optics. The first observation of second-harmonic generation by Peter Frankin [4] and coworkers sparked the beginning of the entire new field of nonlinear optics. Among the first reports of nonlinear refraction were LID tracks in ruby rods due to self-focusing in the medium [5].

One needs only to consider the electric field produced by a very modest Q-switched laser focused to a small spot; for example, a 1 mJ pulse of a 10 ns duration, focused into a 5 μm radius spot, inside a material of refractive index equal to 1.5 produces an electric field in excess of 5.5 mV/cm (root mean square field = RMS). Such an electric field exceeds the threshold needed for dielectric breakdown in many good dielectric materials, including many used to make components for lasers.

1.3 LID: An Electric Field–Dependent Phenomenon

James Clark Maxwell (1831–1879) established that light is electromagnetic radiation. Prior to Q-switched lasers, few phenomena were observed that were a direct manifestation of the electric fields in electric and magnetic (E&M) waves, other than as carriers of energy in the beam. In fact, LID is quite possibly among the first such field-dependent phenomena observed.

RMS electric fields in the megavolt range, bright sparks observed in LID in highly transparent materials, and the law linear absorption in such materials resulted in the conclusion that laser-induced breakdown (LIB) was the mechanism for failure in transparent materials (materials with band gaps in some cases an order-of-magnitude larger than the energy of photons from some lasers) [6]. However, a much simpler—even if perhaps more subtle—observation of the direct relation of the electric field associated with light with LID is the asymmetry observed in the laser damage fluence or irradiance for entrance and exit surfaces of materials.

Consider a typical dielectric window through which a laser beam is propagated. Fresnel reflection loss at air-window entrance surface clearly means that less energy reaches the exit surface of the window (here absorption and scattering losses are small and neglected). A reasonable conclusion is that it would take less laser input to the window to damage the entrance surface than the exit surface. However, the opposite is observed.

This observation was a subject of much speculation for a period of time until Crisp [7] produced the elegantly simple explanation: for a given irradiance into a window, the electric field associated with the beam is *higher* at the exit surface due to the basic fact that the Fresnel reflected field at the entrance surface is 180° out of phase with the incident field, whereas at the exit surface, the reflected field is in phase with the incident field. Thus, the net electric field is *higher* at the exit surface than at the entrance surface for a given input irradiance. The net result is the observed lower damage threshold for the exit surface, as measured in terms of the input irradiance.

This revelation led to much work on what is often called *field enhancement* due to materials defects, surfaces, and optical elements such as multilayer thin film systems where interference of the light field is key to the function of the device. This phenomenon is discussed in great detail in the chapters that follow.

There was a flood of ideas for laser applications following the invention of the ruby laser, including precision measurement, remote delivery of precise amounts of energy, and exotic applications such as laser weapons and laser-driven nuclear fusion for energy generation. Many promising applications, then as now, are limited by LID, either in the lasers themselves or in the various components needed to control and direct the light from the lasers.

1.4 Strategies for Minimizing LID

One simple way to manage problems associated with LID is to reduce the fluence or irradiance by simply expanding the laser beam. However, the cost—as well as weight and volume—increases as the surface area of optical components increases, often in a nonlinear fusion. In many applications, compact systems are essential to the intended use.

One example is the laser source on the Mars exploration vehicle [8]. This remote space craft uses LIB spectroscopy to remotely analyze Martian rocks.

Therefore, practical considerations of cost and compactness often lead to laser systems and applications that are limited by LID to the various optical components associated with the laser systems. This, in turn, has led to international efforts to develop optical components more resistant to LID. Progress in this quest has demanded

1. Focused efforts to develop a fundamental understanding of physical processes that lead to LID
2. The development of measurement techniques to better identify materials characteristics that lead to LID and for the detection and diagnosis of LID events
3. The development of new materials and materials preparation techniques, especially the preparation of damage-resistant precision optical surfaces
4. Advancements in thin film materials and thin film deposition technology

These topics, along with examples of laser applications that are demanding improvement of optical performance, are the subject of the chapters that follow in this book. These topics have also been the focus in the annual symposium on LID to optical materials [8]. Over 40 years of scientific and technological progress are summarized in the proceedings of these meetings. The proceedings are available from the SPIE [9] and are available in searchable format online.

Solutions to the problem of LID are elusive in major part due to the broad scope of laser applications and the demands of various applications. Laser sources span the pulse width from continuous waves to pulses as short as 65 (18 orders of magnitude!) and terahertz region to x-rays (a factor of at least 1000 in photon energies) [10]. To this astronomical parameter space range, one needs to consider a variety of complex linear and nonlinear processes that can affect LID. Some applications demand novel materials for frequency conversation, polarization control and manipulation, beam combining, pulse width control, as well as precision beam pointing and focusing.

Taken together, all these factors make it impossible to answer an often posed question: *What is the LID threshold* (*LIDT*) *of this optical element?* Or, given that a certain optical component is known for a given set of conditions, can one predict or scale to another set of conditions? Experience has shown that precise scaling is speculative at best. (Scaling laws are discussed in Chapter 7.)

1.5 Rule of Thumb for LID Scaling

While detailed scaling of LID is not currently possible, there is a very simple *rule of thumb* for estimating limits imposed by LID [11].

$$E_d = (10\ \text{J/cm}^2)\ (\text{tp}/1\ \text{ns})^{1/2} \tag{1.1}$$

where

E_d is the damage threshold fluence in J/cm^2

tp is the laser pulse width in seconds

This equation gives a reasonable approximation of the LIDT to within plus or minus an order of magnitude for otherwise highly transparent materials over the wavelength range from the ultraviolet (UV) to the infrared spectral region. Laser systems expected to operate with fluences within this range or higher will likely be dominated by LID considerations, whereas fluences below this range will not likely result in LID problems.

There is limited theoretical basis for this rule of thumb except the assumption that in practical situations, LID is most often limited by defects at surfaces and in thin film coatings. Whatever the mechanism for coupling light into these defects, one can conclude that ultimately damage (melting, ablation, cracking, etc.) results from an impulse on energy deposited in a material. Resistance to damage is thus at least in part dependent on the diffusion of the deposited energy.

One should not use Equation 1.1 to predict exact values of LID thresholds, rather, it should only be used as an indicator of expected LID issues. If one needs to know the LIDT to greater precision than offered by Equation 1.1, then one must make careful measurements of the LID for the material system to be used and for the conditions of use (laser pulse width, wavelength, beam spot size, etc.).

References

1. Maiman, T.H., Stimulated optical radiation in http://spie.org/x1848.xmlRuby. *Nature*, 187(4736), 493–494.
2. Bass, M., Professor, CREOL—The College of Optics and Photonics, University of Central Florida, Orlando, FL, Private communication, 2012.
3. McClung, F.J. and Hellwarth, R.W., Giant optical pulsation from ruby. *Journal of Applied Physics*, 33(3), 828–829, 1962.
4. Frankin, P., Hill, A., Peters, C., and Weinreich, G., Generation of optical harmonics. *Physical Review Letters*, 7(4), 118, 1961.
5. Avizonis, P.V. and Farringt, T., Internal self-damage of ruby and ND-glass lasers. *Applied Physics Letters*, 7(8), 205–210, 1965.
6. Yasojima et al., Laser-induced breakdown in ionic crystals and a polymer. *Japanese Journal of Applied Physics*, 7, 552, 1968.
7. Crisp, M.D., in *Damage in Laser Materials*, Glass, A.J. and Guenther, A.H., eds., National Bureau of Standards (US) Special Publication 387, 1973.
8. Lanza, N.L., Wiens, R.C., Clegg, S.M., Ollila, A.M., Humphries, S.D., Newsom, H.E., and Barefield, J.E., Calibrating the ChemCam laser-induced breakdown spectroscopy instrument for carbonate minerals on Mars. *Applied Optics*, 49(13), C211–C217, 2010.
9. Bennett, H.E., Chase, L.L., Guenther, A.H., Newnam, B.E., and Soileau, M.J., *24th Annual Boulder Damage Symposium Proceedings—Laser-Induced Damage in Optical Materials: 1992*, Boulder, CO, September 28, 1992, http://spie.org/x1848.xml.
10. Zhao, K., Zhang, Q., Chini, M., Wu, Y., Wang, X., and Chang, Z., Tailoring a 67 attosecond pulse through advantageous phase-mismatch. *Optics Letters*, 37(18), 3891–3893, 2012.
11. Soileau, M.J., 40 Year retrospective of fundamental mechanisms, *Proceedings of SPIE*, Exarhos, G.J., Ristau, D., Soileau, M.J., and Stolz, C.J., eds., Vol. 7132, pp. 1–14, 2008.

2. Laser-Induced Damage by Thermal Effects

Roger M. Wood

2.1 Introduction

Although most laser scientists instinctively link the term *laser-induced damage threshold* (LIDT) with dielectric breakdown and, thenceforth, quote its value in terms of the peak power density, W cm^{-2}, this is only half the story.

For all but the most highly transparent materials (e.g., fused silica, diamond, quartz, and sapphire), the damage threshold is more likely to be linked to thermal absorption in the laser pulse length region from 10^{-8} s to continuous wave (CW). In this scenario, the onset of damage, whether thought of as melting, catastrophic stress, drilling, or cutting, is related to the melting and/or vaporization of the material. These mechanisms vary between two pulse length–related regimes—the first regime is where the peak temperature is related to a steady-state process and is valid from CW to about 10^{-6} s. The second regime is where the peak temperature is governed by the relative size of the focused spot, the component diameter, and the thermal diffusivity of the sample under test. This second regime is valid for all pulse lengths below 10^{-6} s. However, for highly transmitting materials (e.g., fused silica, diamond, and sapphire), the thermal damage threshold is so relatively high that other damage mechanisms come into play before strict thermal effects take place. These are dielectric breakdown for pulse lengths of ~10^{-8}–10^{-10} s, avalanche ionization for pulse lengths of 10^{-10}–10^{-13} s, and multiphoton absorption for pulse lengths lower than ~10^{-13} s. These mechanisms will be discussed in subsequent chapters.

Laser-Induced Damage in Optical Materials. Edited by Detlev Ristau © 2015 CRC Press/Taylor & Francis Group, LLC. ISBN: 978-1-4398-7216-1.

The aim of this chapter is to allow the calculation of the theoretical maximum irradiation level below which no laser-induced damage (LID) occurs to a perfectly homogeneous material and to give some indication as to why this maximum LIDT is rarely reached in practice.

2.2 Theory

When a light beam is incident on the surface of a material or component, some of the energy is absorbed in the form of heat. The interaction depends on the laser parameters (wavelength, pulse length, and pulse repetition frequency [PRF]); the relative sizes of the beam and the material/component under test; the ambient conditions; the mounting conditions; and the optical, mechanical, and thermal properties of the material/component irradiated. The maximum temperature will normally be at the center of the irradiating beam on the surface of the irradiated material. Thermal damage will normally appear at this point unless the damage is stress related or resulting from localized absorbing imperfections within the material. A simplified schematic of the local peak temperature at the center of the beam on the surface of the material in terms of the pulse temporal shape and PRF is given in Figure 2.1a through e.

For short triangular pulses, see Figure 2.1a, the maximum temperature, at the center of the beam, occurs at or after the peak of the temporal pulse. For square and/or

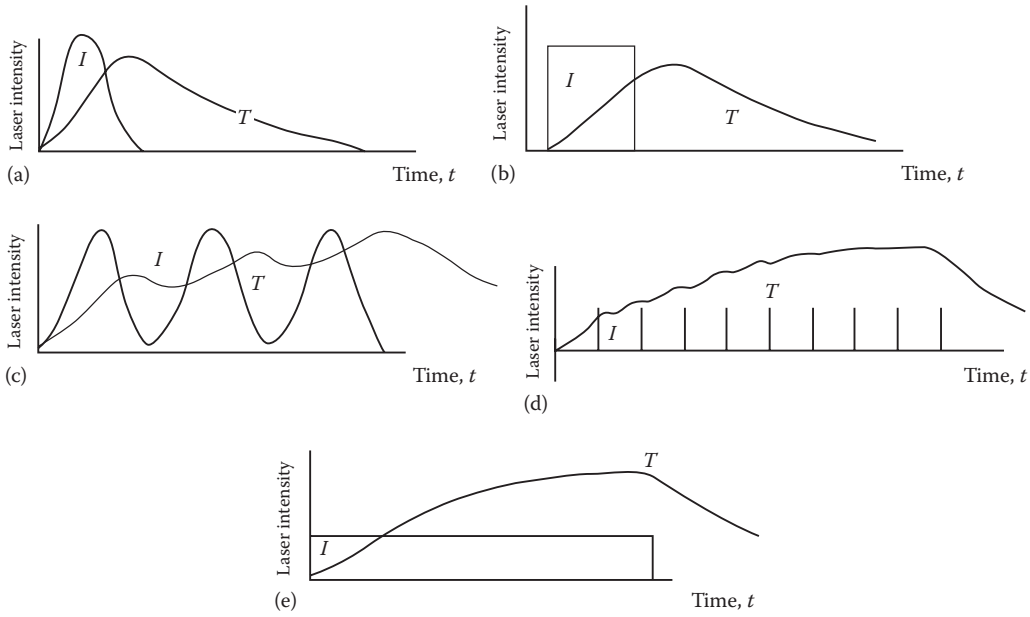

FIGURE 2.1 Laser beam intensity, *I*, and material temperature, *T*, versus time, *t*. (a) Short pulse, (b) long pulse, (c) low PRF pulse train, (d) high PRF pulse train, and (e) CW beam. PRF, pulse repetition frequency; CW, continuous wave. (From Wood, R.M., 2003, *Laser-Induced Damage of Optical Materials*, IOP Publishing/Taylor & Francis Group, Bristol, U.K., 2003.)

long pulses, see Figure 2.1b, the maximum temperature is close to the end of the pulse. For a low repetition series of pulses, see Figure 2.1c, the temperature oscillates in line with the repetition temperature of the sample and gradually rises. For a high PRF train of pulses, the temperature at the center of the sample gradually rises, see Figure 2.1d, and, apart from being slightly more spiky, shows very much the same pattern as the temperature measured for a CW beam, see Figure 2.1e. In all these figures, I stands for the laser beam intensity envelope and T stands for the temperature measured at the surface of the material at the center of the laser beam.

Absorption of energy will give rise to a rise in temperature, leading to thermal expansion, strain, birefringence, movement of internal defects, cracking, melting, and catastrophic shattering. High peak power densities may also give rise to the advent of nonlinear absorption and transmittance, electro-optic effects, second harmonic generation, optical parametric oscillation, and self focusing. These effects may add to the amount of energy absorbed and lower the observed LIDT. A combination of these mechanisms may add up to change the beam shape, induce birefringence, and shatter or melt the component. They can also be put to use to cut, drill, weld, and anneal.

There are four predominant scenarios where thermal damage may be initiated. The first is in transparent and semitransparent materials where the laser energy is deposited in a slightly truncated cylinder. This will apply to most laser window materials and will be highly wavelength sensitive. The second scenario is where the material in question is highly absorbing on the surface of the material and little energy reaches into the material (e.g., in the case of metal mirrors). The third scenario is where there are absorbing inclusions within a semitransparent material (e.g., metal particulates in glass or carbon particulates in diamond) or where there are small, highly mobile grain boundaries, which can move with a rise in temperature and can join together to form thermal barriers with subsequent cracking. There is a fourth scenario that is brought about by nonperfect input surface finish. This is the subject of Chapter 12. The third and fourth scenarios will drop the LIDT from that achieved for a perfect, homogeneous material.

2.3 Heat Transfer in Transparent Materials

When laser radiation is incident in a transmitting medium, it is absorbed in a cylinder, passing through the material on the axis of the laser beam. In the case of a semiabsorbing material, the cylinder changes to a truncated cone. Any absorption in the material at the laser wavelength causes both a temperature rise at the center of this cylinder and a radial strain between this center line and the edge of the component. In most cases, this can be seen as a two-dimensional temperature gradient between the center axis of the laser radiation and the edge of the component. Unless the laser beam is being focused inside the component, LID will occur at the surface of the component under test.

The thermally induced LIDT may therefore be defined as the point where the material surface at the center of the beam reaches the melting point of the material under test, T_m. The temperature rise, the spread of the heat, and the radial strain depend

not only upon the material properties and the amount of heat absorbed but also on the beam diameter, the component diameter, and the laser pulse duration.

$$E_D = C\frac{dT}{\alpha}, \tag{2.1}$$

where
- α is the absorption coefficient of the material at the laser wavelength
- C is the heat capacity of the component
- $dT = T_m - T_a$ is the laser-induced temperature rise, where T_a is the ambient temperature and T_m is the melting point of the material

A threshold for catastrophic cracking can similarly be defined:

$$E_D = \frac{C\kappa S}{\beta\alpha}, \tag{2.2}$$

where
- S is the damaging stress
- β is the volume expansion coefficient

It is useful to define a diffusion length, L, the distance the heat will travel out from the center of the beam in the duration of the laser pulse, τ:

$$L^2 = 4D\tau \tag{2.3}$$

where
- D is the diffusivity ($=\kappa/\rho C$)
- τ is the laser pulse duration
- κ is the thermal conductivity
- ρ is the material density

When the thermal conduction out of the irradiated volume becomes nonnegligible, that is, when

$$\frac{r^2}{\tau} \ll D \ll \frac{R^2}{\tau}$$

where
- r is the laser spot radius
- R is the component radius

This occurs for small radius laser spots, long laser pulse lengths (and high PRF trains of laser pulses), and large component diameters.

The illuminated region can now be treated as a continuous line source (Carslaw and Jaegar 1947).

The energy densities required for melting or catastrophic strain are then given by

$$E_D = \frac{4DCdT \ln\left(4D\tau/r^2\right)\tau}{\alpha r^2} \tag{2.4}$$

or

$$E_D = \frac{4\kappa CDS\tau}{\beta\alpha r^2}. \tag{2.5}$$

It will be seen from these equations that in this temporal regime, the damage threshold will be dependent on the power in the beam rather than on energy density or even on the more conventionally quoted power density.

In the extreme, in the case of long irradiation times (long pulse, multiple pulsing, and CW irradiation), the component temperature gradually rises to a maximum and the equation for the temperature rise, at the point of damage, reduces to

$$dT = T_m - T_a = \frac{P\alpha}{2\rho C\tau\pi D}, \tag{2.6}$$

which is the steady-state temperature profile in a semi-infinite solid (see Figure 2.1d and e).

LIDT will therefore, for long pulse, high-pulse repetition frequency pulse trains and CW irradiation, be governed by the equation

$$\frac{P}{\tau} = \frac{dT 2\rho C\pi D}{\alpha}. \tag{2.7}$$

It will be noted, from perusal of this equation, that the LIDT will be proportional to the linear energy density, W cm^{-1}, if the laser pulse length, τ, is long enough for the heat to be transferred out of the beam center during the irradiation.

When the beam radius is much larger than the diffusion length, that is, $2r > L$, that is, for large laser spot sizes and for short duration pulses, there is negligible spread of the energy in the pulse duration. This means that for short irradiation times the damage thresholds will be pulse length independent. It will therefore be seen that in the short pulse regime the damage threshold is a constant value if expressed in terms of the peak power density, that is, in units of J cm^{-2}.

As should be expected from these equations, the LIDT for thermal damage can be calculated from the material parameters. Table 2.1 lists the expected LIDTs for a range of commonly used laser window materials. It may be noted, from this table, that many of the materials will suffer LID before they reach their true melting points as they exhibit other deleterious effects before they reach that point. For example, most glasses soften at temperatures below the melting point; chlorides, sulfides, and selenides dissociate; diamond graphitizes and all the semiconducting materials suffer from thermal runaway.

Table 2.1 Summary of Thermal Properties of Commonly Used Laser Window Materials

Material	Specific Heat C_p (J g^{-1} K^{-1})	Conductivity K (W cm^{-1} K^{-1})	Density σ (g cm^{-3})	Temperature T_m (°C)	Absorption Coefficient α (cm^{-1})	Thermal Diffusivity D (cm^2 s^{-1})	LIDT CdT/α (J cm^{-2})
1.064 μm							
Fused silica	0.81	0.014	2.21	1610 s	10^{-4}	0.0075	1.1×10^7
BK7	0.86	0.011	2.51	719 s	10^{-3}	0.0051	4×10^5
$LiNbO_3$	0.61	0.046	4.64	1170 m	10^{-2}	0.015	5×10^4
Al_2O_3	0.72	0.46	3.99	2015 m	2×10^{-4}	0.16	7×10^6
Diamond	6.1	22.0	3.51	1000 g	10^{-4}	1.03	6×10^7
				2000 m			1.5×10^8
10.6 μm							
KCl	0.69	0.07	1.99	776 d	10^{-4}	0.047	3×10^6
NaCl	0.88	0.065	2.17	801 d	10^{-4}	0.034	4×10^6
ZnS	0.49	1.72	4.09	700 tr	0.24	0.86	8×10^2
				1830 d			3×10^3

ZnSe	0.3	0.17	5.27	700 tr	0.2	0.11	7×10^2
				1520 d			2×10^3
BaF_2	0.44	0.11	4.89	1280 m	10^{-2}	0.055	4×10^4
CaF_2	0.86	0.095	3.18	1360 m	10^{-2}	0.035	10^5
GaAs	0.27	0.48	5.31	800 tr	2×10^3	0.33	7×10^{-2}
				800 tr	10^{-2}		10^4
				1238 m	10^{-2}		2×10^4
CdTe	0.18	0.075	5.85	1090 m	10^3	0.070	10^{-1}
					10^{-2}		10^4
Ge	0.31	0.67	5.32	370 tr	2×10^{-2}	0.41	5×10^2
				937 m			10^4
Si	0.71	1.68	2.33	1410 m	10^{-2}	1.02	8×10
HgCdTe	0.15	0.10	7.6	930 m	10^3	0.09	10^{-1}

Notes: m, melting point; s, softening point; d, dissociation point; g, graphitization point; tr, onset of thermal runaway.

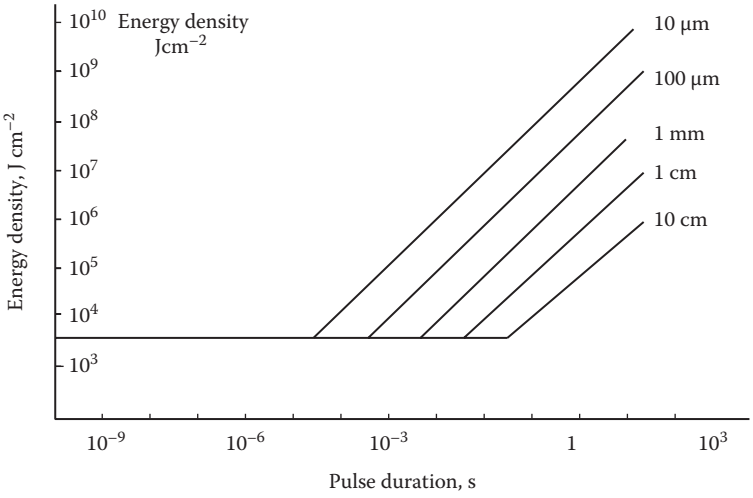

FIGURE 2.2 LIDT (J cm^{-2}) versus pulse length and spot size, ZnSe, 10.6 μm.

The damage thresholds for a ZnSe laser window material, at 10.6 μm, are plotted in Figures 2.2 and 2.3 using different abscissa units. In Figure 2.2, where the damage threshold is quoted in terms of the energy density (J cm^{-2}), it will be seen that the threshold, LIDT, is constant at short pulse lengths and dependent on both spot size and pulse length at longer pulse lengths. Figure 2.3, where the damage threshold is plotted in terms of the linear power density (W cm^{-1}), indicates the opposite. These two figures show that it is necessary, in quoting the damage thresholds of these materials, to be aware that the thermo-mechanical properties of the materials affect the relationship between the pulse length, the pulse energy, and the pulse shape. The break point between the pulse

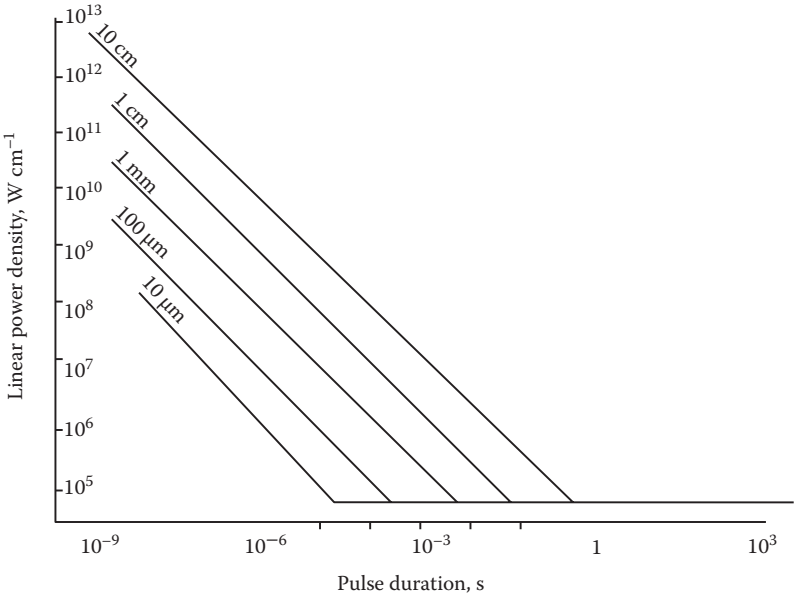

FIGURE 2.3 LIDT (W cm^{-1}) versus pulse length and spot size, ZnSe, 10.6 μm.

Table 2.2 Thermal Nonlinear Break Point

Thermal Diffusivity, D	Uniform Beam Radius, r, or Gaussian Beam 1/e Diameter Pulse Length, τ (s)			
($cm^2\ s^{-1}$)	10 μm	100 μm	1 mm	1 cm
10^{-3}	10^{-3}	10^{-1}	10^{1}	10^{3}
10^{-2}	10^{-4}	10^{-2}	10^{0}	10^{2}
10^{-1}	10^{-5}	10^{-3}	10^{-1}	10^{1}
10^{0}	10^{-6}	10^{-4}	10^{-2}	10^{0}

length-dependent equation (Equation 2.4) and the pulse length-independent equation (Equation 2.1) sections of the energy density versus pulse duration graphs for thermal damage is given by $\tau = r^2/D$. This transition point can be calculated for a range of spot radii and thermal diffusivity values, and these are listed in Table 2.2. The table lists the pulse lengths, τ, at which the transition occurs for a range of thermal diffusivities, D, and laser beam spot radii, r. It should be noted that although the equations have been derived, assuming a square-topped spatial energy density profile of radius, r, they are still correct if the value of the 1/e diameter of a Gaussian beam is substituted.

Figure 2.4 depicts the LIDT versus pulse length for a number of common optical and laser window materials, showing the break point. In practice, the transition is much more

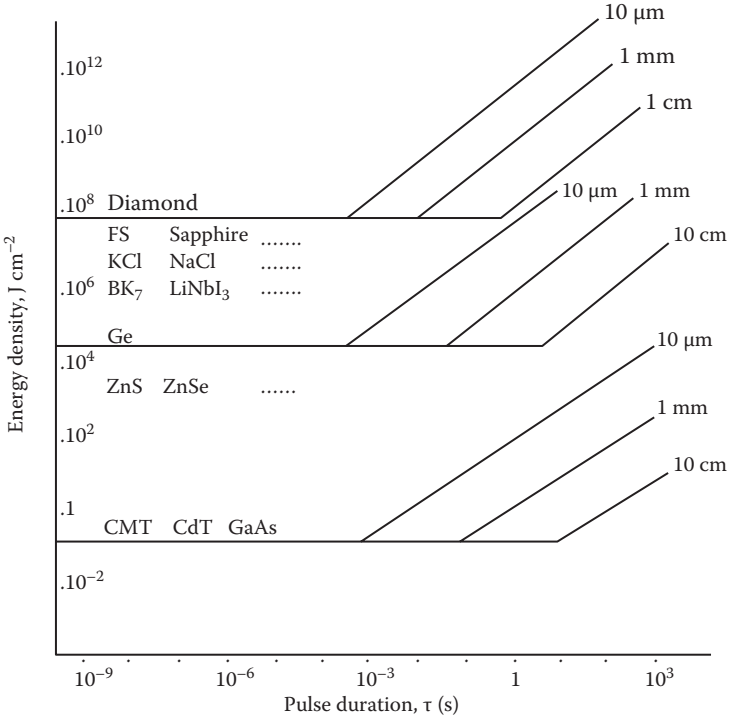

FIGURE 2.4 Thermally induced LIDT (J cm^{-2}) versus pulse duration, τ (s).

curved. It must also be emphasized that these *relatively high LIDTs* are only observed in the highly transmitting region of the wavelength spectrum. Outside the transmission window, the LIDTs become progressively lower as the material absorption increases.

For all the semiconducting materials that form the main class of infrared-transmitting materials (e.g., germanium, zinc selenide, zinc sulfide, gallium arsenide, mercury cadmium telluride, etc.), it should be noted that thermal runaway occurs at fairly low temperatures, compared to the melting point (see Table 2.1). In practice, this means that the value for T_m in Equations 2.1 and 2.6 is a low value, the point at which thermal runaway starts, and not the true melting point of the material.

It should be noted that the only common infrared-transmitting materials that do not suffer from thermal runaway are the halides. As long as these materials are kept in a strictly dry environment, they exhibit relatively high LIDTs, which do not drop with laser PRF. However, they are all hygroscopic and, if left in the open, absorb water vapor, which then both dissolves the substrate and absorbs infrared radiation.

2.4 Absorbing Materials

When a laser beam is incident on a nontransmitting metallic surface, a small amount of radiation penetrates it to a distance called the skin depth, which is in turn a function of the electrical conductivity. Subsequent absorption of this radiation by free carriers within the material raises the temperature of the surface. As the temperature rises, stress and distortion of the surface will occur. In the limit, catastrophic damage may occur due to mechanical failure, to melting of the surface, or to a combination of both.

The temperature rise due to absorption of energy may be calculated using a one-dimensional heat flow calculation. At the center of the beam, the temperature rise, dT, is given by

$$dT(x,t) = 2\alpha I_o \frac{t}{\pi\kappa\rho C} \operatorname{ierfc} \frac{x}{2\sqrt{\kappa t/\rho C}}, \tag{2.8}$$

where

t is the irradiation time
α is the absorption
I_o is the peak intensity of the beam
κ is the thermal conductivity
ρ is the density of the material
x is the depth at which the measurement takes place ($x = 0$ at the surface)

As long as the function ierfc(y) is small ($y > 2$), a sample thickness of $x > 4\sqrt{\kappa t/\rho C}$ is effectively infinitely thick as regards the effect on the maximum surface temperature. This leads to the expression

$$dT(t) = \frac{2\alpha I_o \sqrt{t}}{\sqrt{\pi\kappa\rho C}} \quad \text{at } x = 0. \tag{2.9}$$

If damage is due to surface melting, then

$$dT = T_m - T_a,$$

where

T_m is the temperature at which the surface melts
T_a is the ambient temperature

It should be noted that the absorption is the sum of the intrinsic absorption and the surface absorption. It has been proved that the roughness of the surface of a metal mirror affects the absorption. It should be noticed however that the roughness needs to be measured in terms of the wavelength of the incident laser radiation.

The expression $(T_m - T_a)\sqrt{\kappa\rho C}$ may be regarded as a figure of merit (FOM) for LID of metal surfaces. It may however be modified by anomalous absorption of the sample at the wavelength of interest. A table containing this FOM, with respect to copper, for a range of metal mirror candidates for use at 10.6 μm, is shown as Table 2.3. It should be recognized that all the constants involved may be temperature dependent. The thickness

Table 2.3 Figure of Merit for 10 μm Mirror Candidate Materials

Element	T_m (°C)	κ (W cm^{-1} K^{-1})	ρ (g cm^{-3})	C (J g^{-1} K^{-1})	FOM wrt Copper
Copper	1084	4.01	8.96	0.385	1.000
Aluminum	660	0.243	2.7	0.90	0.124
Beryllium	1287	2.00	1.85	1.825	0.832
Chromium	1907	0.937	7.15	0.449	0.827
Gold	1064	3.17	19.3	0.129	0.741
Hafnium	2233	0.230	13.3	0.144	0.371
Molybdenum	2623	1.38	10.2	0.251	1.236
Nickel	1455	0.907	8.9	0.444	0.400
Niobium	2477	0.537	8.57	0.265	0.234
Osmium	3033	0.876	22.5	0.130	1.219
Palladium	1555	0.718	12.0	0.246	0.565
Platinum	1768	0.716	21.5	0.133	0.632
Rhenium	3186	0.479	20.8	0.137	0.934
Rhodium	1964	1.50	12.4	0.243	1.044
Ruthenium	2334	1.17	12.1	0.238	1.356
Silver	962	4.29	10.5	0.235	0.774
Tantalum	3017	0.575	16.4	0.140	0.870
Titanium	1668	0.219	4.5	0.523	0.299
Zirconium	1855	0.227	6.52	0.278	0.324

Source: Lide, D.R., *CRC Handbook of Chemistry and Physics*, CRC Press, Boca Raton, FL, 1994.

of any coating, dielectric or metallic, will also affect the LIDT. In the case of a coated substrate (e.g., a gold-coated copper mirror), if the coating thickness is much less than $\sqrt{\kappa\tau/\rho C}$, then the values for κ, ρ, and C are determined by the substrate material, while the value for α is that of the coating material and T_m is the lower of the melting points of the two materials.

Taking into account the correction that has to be made if the laser pulse is not square, the LIDT is given by

$$T_m - T_a = dT = \frac{I_o \alpha}{2\sqrt{\pi\rho\kappa C}} f(t), \tag{2.10}$$

where $f(t)$ is a time-dependent function, the precise form of which is determined by the input pulse shape. This is discussed in more detail in Wood (2003).

Note that the LIDT is inversely proportional to the temperature of the material under test and that it can therefore be raised by back cooling the substrate.

It is now necessary to consider when the peak temperature on the center axis of the laser beam reaches a maximum. The equation of the temperature curve can be approximated by

$$\Delta T = \frac{P\alpha}{2\rho C r \pi D} \operatorname{erfc} \frac{r}{\sqrt{4Dt}},$$

where P is the power of the laser beam, W, which, for large values of t, reduces to

$$\Delta T = \frac{P\alpha}{2\rho C r \pi D},$$

which is, again, the steady-state radial profile of the temperature in a semi-infinite solid.

It will be realized that the temperature of the material is inversely proportional to the radial distance, r, from the center of the beam.

For short, single pulses, the temperature rise is proportional to the incident energy density, that is, for short, single pulses, the LIDT is a constant when expressed in terms of J cm^{-2}.

When the pulse duration is longer than the material heat diffusion constant, that is, when the heat has time to diffuse out of the irradiated spot, the damage threshold becomes constant when measured in terms of W cm^{-1}.

The two scenarios discussed earlier can be seen easiest when the LIDT of an oxygen free high conductivity (OFHC) copper mirror sample is plotted versus the laser pulse duration (see Figures 2.5 and 2.6). It will be noticed that the shapes of these graphs are identical with those generated for transmitting materials.

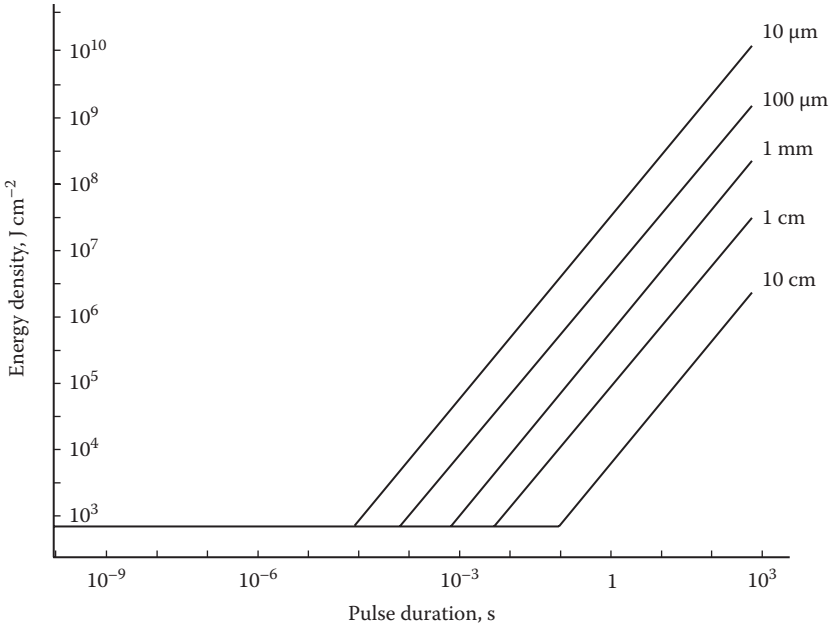

FIGURE 2.5 LIDT (J cm^{-2}) versus pulse duration, τ, and spot size, *r*. OFHC copper at 10.6 μm.

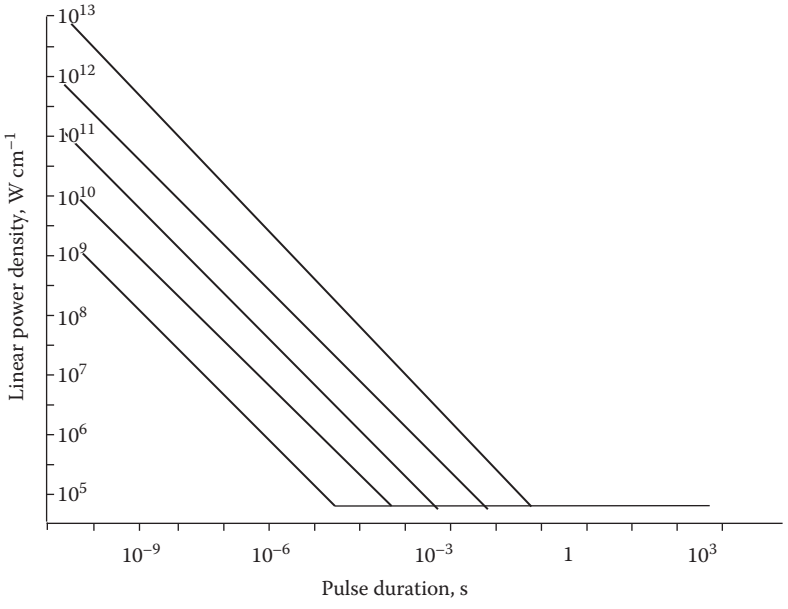

FIGURE 2.6 LIDT (W cm^{-1}) versus pulse duration, τ, and spot size, *r*. OFHC copper at 10.6 μm.

2.5 Influence of Inclusions

There are two major scenarios where LIDT is influenced by the local material properties rather than by the average thermo-mechanical properties.

The first scenario is where there are localized absorbing specks of material within the lattice of a transparent or semitransparent material. The heat absorbed is a function of the speck cross section. When the speck is large, $r > 100$ μm, the temperature rise averages out over the surface of the speck and is easily transmitted to the transparent lattice. In this case, although the optical quality of the material is compromised, the absorption rarely causes damage. When the speck is of the order of 10–0.1 μm, the particle will absorb the radiation and damaging stress is likely to build up between the absorbing speck and the surrounding lattice due to the thermal expansion of the speck. A theoretical treatment has predicted the critical radius to be 0.4 μm for laser pulses in the ns pulse length range (Koldunov et al. 2002). When the particle size is <0.1 μm, any absorption will only add to the absorption and damage is unlikely to occur (Duthler and Sparks 1973).

This has been observed in the case of platinum or tungsten particles originating from the crucibles in which glass or Nd:YAG laser crystal has been melted. In this case, the speck was seen to have melted and exploded, leaving craters inside the bulk material. Another instance of absorbing speck has been observed inside substandard chemical vapor deposition (CVD) grown diamond window material. A third example is that of carbonization of thin glue layers used in cementing optical filters and/or dielectric polarizers. In all these cases, the absorption first causes melting/evaporation or carbonization and this leads to unacceptably high levels of stress and to catastrophic cracking.

The second scenario involves the movement of microscopic grain boundaries inside laser/optical crystals under steady and/or high PRF irradiation. This has been observed in germanium laser window crystal and in CVD-grown diamond. In both cases, the crystal showed little or no deterioration of transmittance during continuous irradiation until, quite suddenly, the crystal split in a circular ring round the laser entry point. In the case of the germanium window, there was evidence of melting at the center of the circular damage ring. In the case of the diamond substrate, the thermal conductivity suddenly underwent a sharp drop at this point (Sussman et al. 1993).

2.6 Discussion

Many laser engineers have been used to measure, and quote, the laser damage thresholds of their optical/laser materials in terms of W cm^{-2} because they are thinking in terms of dielectric breakdown under pulsed irradiation. It took many years, and the incidence of 10.6 μm, CO_2 lasers, for the realization that for all but highly transmitting materials, the damage mechanism might be melting and that in that case the units of measurement should be in terms of J cm^{-2}. It was only fairly recently realized that there was another commonly experienced regime—that of the long pulse, the high repetition rate train of pulses, and CW. In this temporal regime, it was noted early on that the laser damage level was constant for pulses longer than a few seconds, but it was not realized that the steady-state temperature could not be stated in terms of J cm^{-2} for many years. It was only realized that there was a serious problem with quoting the LIDT in terms of the peak energy density for long pulses and CW radiation when the use of beam scanners,

fabricated from beryllium, was promoted because of the lightness of this material. The concern came about because of the extreme toxicity of Be vapor. An analysis of the LIDT showed that if the safe power loading was calculated in terms of J cm^{-2} for small spot sizes, then it could be catastrophic if the laser spot size was increased under the impression that the component could withstand higher laser powers at the same energy density, instead of making the calculations at W cm^{-1} (Wood 1997).

Although the use of W cm^{-1} measurement units had been cautiously highlighted some years previously (Wood 1986) (as very few people were really interested in CW testing at this stage), it came into focus when, in the process of an industry/university cooperative program, the results showed that the damage thresholds of zinc selenide window material under CW testing at 10.6 μm exhibited a constant value of 3000 W mm^{-1} (Greening 1994, 1997).

It has frequently been argued that LIDTs must be proportional to either the power or the energy density (i.e., either measured in terms of J cm^{-2} or in terms of W cm^{-2}) as the eye damage thresholds are measured in these units. This argument does not hold water once it is realized that all eye damage threshold measurements are quoted for a fixed iris diameter. If the diameter of the spot is left out of the calculation, then the parameter of interest is the power, W, and the Electrochemical Commission (IEC) standard does predict that the LIDT for CW beams is a constant power level. The same problem arises with safety goggles and with laser safety screens. If a preliminary damage measurement is made using a CW beam focused down to a small spot, then if the spot size is increased (i.e., allowance is made for defocusing the beam), the assumed safety level, scaled in terms of W cm^{-2}, is soon far above the true safety level, scaled using W cm^{-1}.

References

Carslaw, H.S. and Jaegar, J.C., 1947, *Conduction of Heat in Solids*, Oxford, U.K.: Clarendon Press.

Duthler, C.J. and Sparks, M., 1973, *Theory of Material Failure in Crystals containing Infrared Absorbing Inclusions*. NBS Special Publication, 387, pp. 208–216.

Greening, D., 1994, *Optics and Laser Engineering*, April, p. 25; 1977, *Optics and Laser Engineering*, June, p. 41.

Koldunov, M.F., Manenkov, A.A., and Pokotilo, I.L., 2002, Mechanical damage in transparent solids caused by laser pulses of different durations. *Quantum Electronics* 32, 335–340.

Lide, D.R., 1994, *CRC Handbook of Chemistry and Physics*, Boca Raton, FL: CRC Press.

Sussman, R.S., Scarsbrook, G.A., Wort, C.J.H., and Wood, R.M., 1993, Laser damage testing of CVD grown diamond windows. *Conference on Diamond, Diamond-Like and Related Coatings*, Albufeira, Portugal.

Wood, R.M., 1986, *Laser Damage in Optical Materials*, Bristol, U.K.: Adam Hilger.

Wood, R.M., 1997, Laser induced damage thresholds and laser safety levels. Do the units of measurement matter? *Journal of Optics and Laser Technology* 29(8), 517–522.

Wood, R.M., 2003, *Laser-Induced Damage of Optical Materials*, Bristol, U.K.: IOP Publishing/Taylor & Francis Group.

3. Defect-Induced Damage

Semyon Papernov

Laser-Induced Damage in Optical Materials. Edited by Detlev Ristau © 2015 CRC Press/Taylor & Francis Group, LLC. ISBN: 978-1-4398-7216-1.

3.1 Introduction

Ever since the appearance of a laser as a tool that permits extreme spatial and temporal concentration of light energy, it has been realized that localized absorbing defects in optical components are a major source of laser-induced damage. There is ongoing continuous effort to reduce the number and size of absorbers in optical materials used for laser applications. Still, with ever-increasing laser power densities (for instance, in laser fusion facilities), even nanoscale absorbing defects continue to be a major source of damage.

In this chapter, we consider physical processes that describe the interaction of pulsed-laser radiation with transparent dielectric materials containing isolated absorbing defects in the form of particles made of homogeneous material. Such an interaction has two main aspects in relation to laser damage: First, laser-energy absorption generates thermal and mechanical effects, like heating, melting, evaporation, and fracturing of the host material. The second aspect is that the light field of the laser pulse can be amplified in the vicinity of the absorbing or structural defect, which consequently affects modification of the host material.

The main part of this chapter is devoted to an analysis of thermomechanical processes, and effects of light intensity amplification are addressed toward the end in a special paragraph. First, laser-damage criterion based on reaching a critical temperature is introduced. The effects that the optical and thermal properties of both the defect and host material, along with defect size and shape, have on damage thresholds are considered within the thermal diffusion model. The damage-threshold pulse-length scaling is also evaluated within the thermal diffusion model's framework. These results are compared with experimental data and results of numerical simulations taking into account field enhancement, thermal stresses, and phase transitions for damage initiated by metallic and dielectric defects.

Special consideration is given to the concept of absorption delocalization during the laser pulse for absorbers much smaller than a laser wavelength and related thermal explosion theory. Mechanisms of the free-electron formation in the defect-surrounding material and experimental verification of absorption delocalization using model systems with well-characterized metallic particle absorbers are discussed.

The majority of the processes considered take place during the laser pulse (timescale ~10^{-11} to 10^{-8} s) and consequently describe the state of matter during energy deposition. On the other hand, the damage process also has a second stage characterized by material melting, evaporation, and (in the case of brittle materials) cracking that may continue to evolve after the end of the laser pulse and defines the final damage morphology. In the bulk, the extent of damage is usually defined by the size of cracks formed during the cooling stage. We discuss conditions for crack formation and the effects of pulse length and absorber size.

When a defect located near the surface initiates damage, the damage morphology usually takes the form of a crater. The crater size may be linked to the defect depth using simple scaling relations. Effects of spallation caused by a shock wave originating at the defect location, as well as the difference in energy deposition for the two cases of front (free-surface side) and back irradiation will be considered here.

For most topics presented in this chapter, the assumption is made that the electric field of the light wave outside the absorber is the same as the electric field of the wave inside the homogeneous dielectric host material. Exceptions to this are made only for the few cases of numerical modeling. In fact, this field can be significantly larger in the vicinity of the structural defect, which could be either an absorber in the bulk or differently shaped and oriented surface cracks. We concentrate our analysis here on the effect of the light intensification and its relative role in extrinsic and intrinsic mechanisms of damage.

Localized absorbing defects exist in real optical materials as an ensemble characterized by distributions of sizes, geometry, optical properties, and other parameters. As a result, laser damage initiated by an ensemble of localized defects is probabilistic by its nature, and the probability of damage is linked to the probability of finding a defect within the laser beam area where the fluence exceeds the damage threshold. Consequently, it leads to the beam spot size dependence of the damage probability and related damage threshold. We discuss how damage probability studies can provide information on defect densities and, in some cases, on the defect's optical properties.

The chapter closes with considering laser conditioning as a method for improving the damage resistance of materials containing absorbing defects.

3.2 Thermal Diffusion Model of Absorbing Defect-Induced Damage

3.2.1 Damage Criterion

Modeling of laser-induced damage requires establishing a damage criterion, usually reaching some fixed value by an important damage process parameter. As an example, it could be thermal stress equal to or exceeding the strength of the material, or reaching some critical temperature. Historically, it has been the temperature of the defect-surrounding material reaching a melting point that was considered the decisive event establishing damage. Justification for such criterion in the case of transparent dielectric materials lies in fact that close to this point, structural changes are accompanied by a loss in transparency (band-gap collapse). One can argue that it might be insufficient to create irreversible changes in the optical properties of the material, but, in most cases, it allows one to predict damaging laser intensities and establish important rules governing the damage process.

3.2.2 Heat Equation and Boundary Conditions

The study of localized absorber-driven damage considering energy transfer from a laser-heated defect to the host material by heat conduction was first performed by Hopper and Uhlmann (1970) for the case of metallic absorbers and then explored by other authors (Walker et al., 1981; Lange et al., 1982, 1984; Fuka et al., 1990; Feit and Rubenchik, 2004a)

for absorbers with different thermal and optical properties and various geometries. We consider here a spherical absorber inside an infinite transparent material. The energy of laser radiation is deposited linearly inside the absorber, and then, the heat diffuses from the absorber into the host material. The boundary between the absorber and the host is assumed to be perfect (no thermal resistance). The heat equation for spherically symmetric problem then takes the following form (Fuka et al., 1990):

$$\frac{1}{D_a}\frac{\partial T_a}{\partial t} = \frac{1}{r^2}\frac{\partial}{\partial r}\left(r^2\frac{\partial T_a}{\partial r}\right) + \frac{A}{K_a} \quad 0 \le r \le a \tag{3.1}$$

$$\frac{1}{D_h}\frac{\partial T_h}{\partial t} = \frac{1}{r^2}\frac{\partial}{\partial r}\left(r^2\frac{\partial T_h}{\partial r}\right) \quad r > a, \tag{3.2}$$

where

a is the radius of the sphere
T is the temperature
t is the time
r is the radial distance from the sphere center
D is the thermal diffusivity
K is the thermal conductivity
A is the heat source term (heat generated in unit volume per unit time)
The subscript a denotes absorber and h denotes host material

The interface between the absorber and the host is characterized by the boundary conditions

$$T_a(a) = T_h(a) \quad \text{and} \quad K_a\left(\frac{\partial T_a}{\partial r}\right)_{r=a} = K_h\left(\frac{\partial T_h}{\partial r}\right)_{r=a}$$
$$T_a(r, t=0) = T_h(r, t=0) = 0. \tag{3.3}$$

An exact solution for the temperature $T(r = a, t = \tau)$ at the end of the rectangular pulse τ with constant intensity I (W/cm^2) using Equations 3.1 and 3.2 with these boundary conditions was derived by Goldenberg and Trantor (1952) and has a rather complex integral form:

$$T = \frac{3\sigma I}{4\pi a K_a}\left[\frac{1}{3}\frac{K_a}{K_h} - \frac{2b}{\pi}\int_0^\infty \exp\left(\frac{-y^2\tau}{\delta}\right)F(y)\,dy\right]$$
$$F(y) = \frac{(\sin y - y\cos y)\sin y}{y^2\left[(c\sin y - y\cos y)^2 + b^2y^2\sin^2 y\right]} \tag{3.4}$$
$$\delta = \frac{a^2}{D_a}; \quad b = \frac{K_a}{K_h}\sqrt{\frac{D_h}{D_a}}; \quad c = 1 - \frac{K_h}{K_a},$$

where σ is absorption cross section.

Solving the heat diffusion problem can be simplified (Chan, 1975; Feit and Rubenchik, 2004a), assuming that energy is homogeneously deposited inside the absorber, which is valid for very small, strong absorbers (radius is comparable to a skin depth; metals) and larger, weak absorbers (dielectrics). Consequently, as a reasonable approximation, the temperature inside the absorber can be considered homogeneous. This allows simple expression for the boundary condition that follows from energy conservation considerations: The energy deposited inside the absorber must be equal to increase in the absorber heat content plus heat leaving the surface of the absorber:

$$\gamma I(t) = \frac{4}{3}\rho_a C_a a\left(\frac{\partial T}{\partial t}\right)_{r=a} - 4K_h\left(\frac{\partial T}{\partial r}\right)_{r=a}, \tag{3.5}$$

where

γ is the absorptivity ($\gamma = \sigma/\pi a^2$, σ is the absorption cross section)
I is the light intensity
ρ_a is the mass density
C_a is the heat capacity of the absorber

Solving Equation 3.2 with boundary conditions (Equation 3.5) gives a simple expression (Chan, 1975) for the temperature of the absorber heated by a rectangular pulse of duration τ:

$$T = \frac{\gamma F_a}{4K_h\tau}\left[1 - \exp\left(-\frac{4D\tau}{a^2}\right)\right], \tag{3.6}$$

where

F is the laser fluence (J/cm^2)
$D = 3K_h/4\rho_a C_a$ is the effective diffusivity

In Figure 3.1a, the temperature is plotted as a function of absorber size normalized by the effective diffusion length $2\sqrt{D\tau}$.

One can see that there is an absorber size most susceptible to heating. A qualitative physical explanation for homogeneously heated absorbers is that for very small absorbers a high surface-to-volume ratio leads to efficient heat removal by heat conduction. For large absorbers, absorption cross-section scales (see Section 2.4.2) as a^2, but the volume as a^3, which leads to reduced absorbed energy per unit volume and lower temperatures. Consequently, the most efficient heating might be expected for some intermediate absorber size. At a fixed pulse length, it follows from Equation 3.6 that an absorber subjected to a maximum heating has a radius approximately equal to the effective thermal diffusion length, $a = 1.8\sqrt{D\tau}$. A corresponding temperature T_{max} can be calculated using Equation 3.6:

$$T_{max} = \frac{0.32\gamma F}{K_h}\sqrt{\frac{D}{\tau}}. \tag{3.7}$$

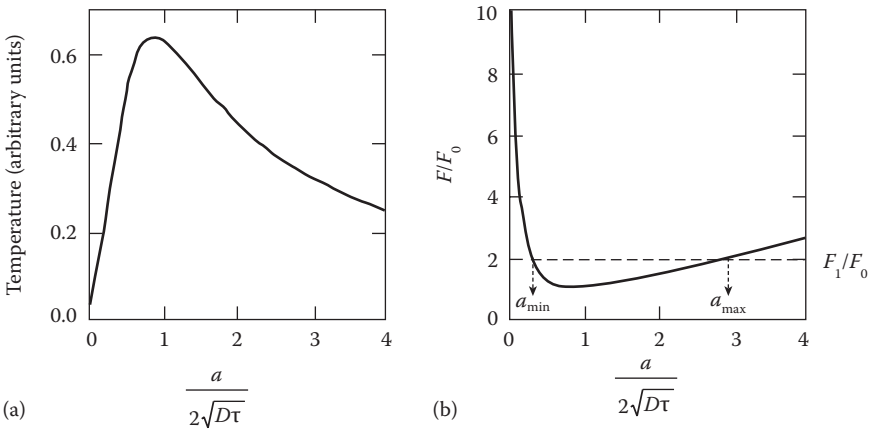

FIGURE 3.1 (a) Absorber temperature and (b) normalized threshold as a function of normalized absorber radius. (Reprinted figure with permission from Feit, M.D. and Rubenchik, A.M., Implications of nanoabsorber initiators for damage probability curves, pulse length scaling, and laser conditioning, in *Laser-Induced Damage in Optical Materials: 2003*, G.J. Exarhos, A.H. Guenther, N. Kaiser, K.L. Lewis, M.J. Soileau, and C.J. Stolz, eds., Vol. 5273, pp. 74–82, SPIE, Bellingham, WA. Copyright 2004 by SPIE.)

Assuming that T_{max} equals the critical temperature of the material, T_{cr}, the damage-threshold fluence F_0 takes the form

$$F_0 = \frac{3.1 T_{cr} K_h \sqrt{\tau}}{\gamma \sqrt{D}}. \tag{3.8}$$

Normalized to F_0, damage threshold versus normalized absorber size dependence (Feit and Rubenchik, 2004a) is plotted in Figure 3.1b. For each fluence $F > F_0$, there is a range of the defect sizes $a_{min} < a < a_{max}$ for which the host material is expected to fail. The resulting damage density may be found by integrating the absorber density between sizes a_{min} and a_{max}. The temperature behavior for the Gaussian pulse shape, $I = I_0 \exp[-(t/\tau)^2]$, with the fluence defined as $F = I_0 \tau$, is very similar to the case of the rectangular pulse, and Equations 3.7 and 3.8 hold (Feit and Rubenchik, 2004a).

3.2.3 Pulse-Length Scaling

The threshold fluence given in Equation 3.8 scales as $\sqrt{\tau}$, the result frequently used to quickly compare the threshold measurements performed with different pulse lengths. Strictly speaking, this result is valid only when absorptivity γ is not size dependent. An exact calculation (Bonneau et al., 2001) of absorptivity as a function of the absorber's size using Mie's theory (Mie, 1908; Bohren, 1983) for metallic absorbers embedded in SiO_2 is shown in Figure 3.2a. One finds strong changes in absorptivity for absorbers smaller than ~200 nm for a 1053 nm wavelength and smaller than ~60 nm for a 351 nm wavelength. For weak absorbers, like SiO, absorptivity is a weakly increasing function of the size (Feit and Rubenchik, 2004a). In the latter case,

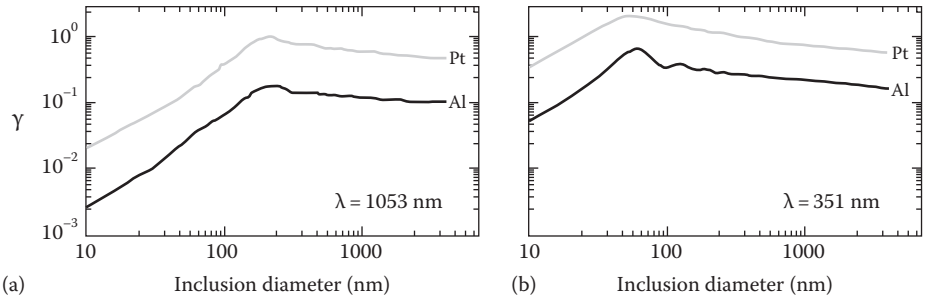

FIGURE 3.2 Metal particle absorptivity as a function of particle diameter for (a) λ = 1053 nm and (b) λ = 351 nm. (Reprinted figure with permission from Bonneau, F., Combis, P., Vierne, J., and Daval, G., Simulations of laser damage of SiO_2 induced by a spherical inclusion, in *Laser-Induced Damage in Optical Materials: 2000*, G.J. Exarhos, A.H. Guenther, M.R. Kozlowski, K.L. Lewis, and M.J. Soileau, eds., Vol. 4347, pp. 308–315, SPIE, Bellingham, WA. Copyright 2001 by SPIE.)

using a simple approximation $\gamma \sim a^q$, where $q < 1$, the threshold fluence scaling has a power coefficient that is always less than 0.5:

$$F_0 \sim \tau^{(1-q)/2}. \tag{3.9}$$

The pulse-length scaling given in Equations 3.8 and 3.9 assumes a broad distribution of absorber sizes, including those most susceptible to heating. In this case, the damage threshold is defined by the failure fluence for the most susceptible absorber. As an example, for absorbers in fused silica and effective diffusivity equal to that of fused silica, $D = 0.008$ cm²/s, and pulse length $\tau = 1$ ns, the most dangerous absorber has a radius $a \approx 50$ nm. Obviously, with increasing pulse length, the size of the absorber that causes failure also increases. Figure 3.3 provides an example of threshold fluence

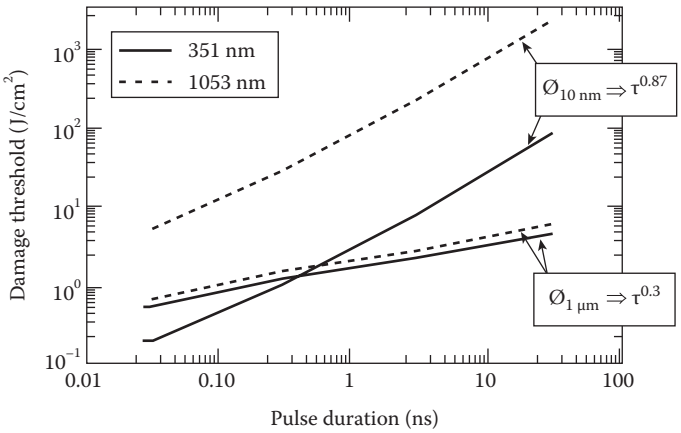

FIGURE 3.3 The 351 nm and 1053 nm damage thresholds as a function of pulse duration for 10 nm and 1000 nm Al-particle sizes. (Reprinted figure with permission from Bonneau, F., Combis, P., Vierne, J., and Daval, G., Simulations of laser damage of SiO_2 induced by a spherical inclusion, in *Laser-Induced Damage in Optical Materials: 2000*, G.J. Exarhos, A.H. Guenther, M.R. Kozlowski, K.L. Lewis, and M.J. Soileau, eds., Vol. 4347, pp. 308–315, SPIE, Bellingham, WA. Copyright 2001 by SPIE.)

numerical calculations (Bonneau et al., 2001), using a thermal diffusion model for Al absorbers and taking into account the temperature dependencies of all important parameters (absorptivity, thermal conductivity, etc.). Here, a different pulse-length scaling exists for 10 and 1000 nm Al absorbers. Note that for metallic absorbers with diameters much larger than skin depth, an assumption of homogeneous absorption is not valid. For such absorbers, energy is deposited in only the layer adjacent to the surface, and heat diffusion initially takes place inside the absorber, leading to changes in the pulse-length scaling.

The scaling for absorbers much smaller or much larger than diffusion length can be predicted qualitatively by considering their temporal heating behavior (Feit et al., 2001b). Small absorbers very quickly reach thermal equilibrium when energy deposition is balanced by the conductive heat removal. This means that the peak temperature will be defined mainly by laser intensity. Consequently, damaging fluence $F = I \cdot \tau$ scales linearly with the pulse length. For very large absorbers, nearly all deposited energy goes into absorber heating (heat removal is small) and peak temperature depends roughly on the total absorbed energy. This results in a threshold fluence being independent of pulse length. Frequently observed $\sqrt{\tau}$ threshold scaling corresponds to an intermediate case of absorbers whose size is comparable to the diffusion length. The 1053 nm damage-threshold measurements for superpolished fused silica and calcium fluoride surfaces (Stuart et al., 1995) (see Figure 3.4a) provide an example of $\sqrt{\tau}$ scaling in the 20 ps to 1 ns pulse-length range. Figure 3.4b shows similar $\tau^{0.4:0.5}$ scaling obtained for fused-silica surfaces in earlier 1064 and 355 nm measurements (Campbell et al., 1991) covering a pulse range from 100 ps to 50 ns. Numerical calculations (Feit et al., 2001b) using

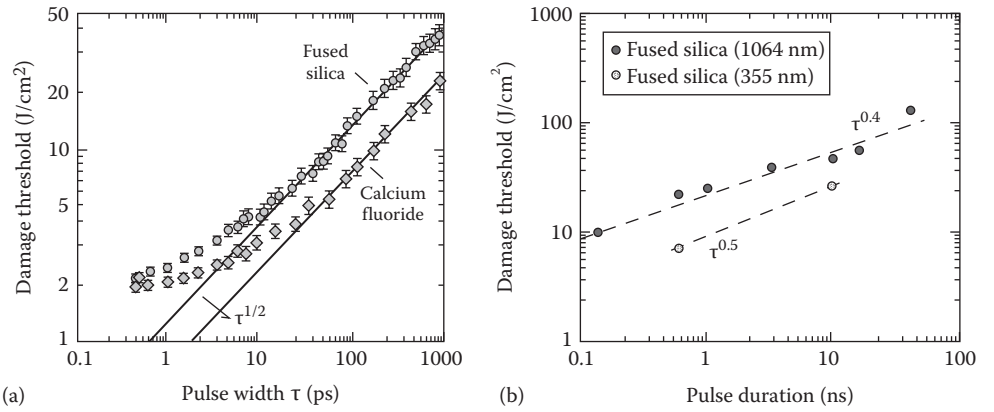

FIGURE 3.4 (a) Damage threshold as a function of pulse duration for fused silica and calcium fluoride, λ = 1053 nm. (Reprinted figure with permission from Stuart, B.C., Feit, M.D., Rubenchik, A.M., Shore, B.W., and Perry, M.D., Laser-induced damage in dielectrics with nanosecond to subpicosecond pulses, *Phys. Rev. Lett.*, 74, 2248–2251. Copyright 1995 by the American Physical Society.) (b) Damage threshold as a function of pulse duration for fused silica, λ = 355 nm, 1064 nm. (Reprinted figure with permission from Campbell, J.H., Rainer, F., Kozlowski, M.R., Wolfe, C.R., Thomas, I.M., and Milanovich, F.P., Damage resistant optics for a megajoule solid state lasers, in *Laser-Induced Damage in Optical Materials: 1990*, H.E. Bennett, L.L. Chase, A.H. Guenther, B.E. Newnam, and M.J. Soileau, eds., Vol. 1441, pp. 444–456, SPIE, Bellingham, WA. Copyright 1991 by SPIE.)

an exact solution of the thermal equations and hypothetical absorber size distribution dominated by small absorbers resulted in a scaling with a power of 0.35–0.45, which appears to be in very good agreement with the experimentally observed $\tau^{0.35}$ damage-threshold scaling for potassium dihydrogen phosphate (KDP) crystals (Runkel et al., 2000).

In the preceding analysis of pulse-length scaling, absorptivity was considered as a temperature-independent parameter. In fact, temperature dependence (known for the number of optical materials) may lead to thermal instability in a form of nonlinear temperature growth, the so-called thermal explosion (Danileiko et al., 1978; Koldunov et al., 1990, 1996). We will consider this damage mechanism later (see Section 3.3) but, in the context of pulse-length scaling, one might expect different kinetics of absorber heating and consequently different scaling. In this case, the absorber may be characterized by some critical temperature T_{cr} above which the temperature growth cannot be balanced by heat diffusion. A solution of heat equations similar to Equations 3.1 and 3.2 with boundary conditions given by Equation 3.5 (homogeneous absorption) and temperature-dependent absorptivity $\gamma = \gamma(T)$ leads to the following threshold intensity scaling for a rectangular pulse (Koldunov et al., 1996):

$$I_{th}(\tau) = \frac{I_{cr}}{1 - \exp(-\tau/2\tau_0)}, \tag{3.10}$$

where

$I_{cr} = I_{cr}(T_{cr})$ is the threshold intensity at $\tau \gg \tau_0$

$\tau_0 = \rho_a C_a a^2/3K_h$ is the absorber temperature's relaxation time

It should be noted here that Equation 3.6, after substituting intensity I for F/τ, takes on a functional expression very similar to Equation 3.10. For short pulses when $\tau \ll \tau_0$, Equation 3.10 reduces to the form

$$I_{th}(\tau) = \frac{2\tau_0}{\tau} I_{cr}. \tag{3.11}$$

It follows from Equation 3.11 that in this case, damage threshold is characterized by fluence F_{th} (energy density):

$$F_{th} = \tau I_{th}(\tau) = 2\tau_0 I_{cr}. \tag{3.12}$$

The threshold pulse-length curves calculated using Equation 3.10 for rectangular pulses and numerical calculations for a Gaussian temporal pulse shape (Koldunov et al., 1996) are shown in Figure 3.5. These curves, calculated using τ_0 as the only adjustable parameter, are in good agreement with experimental data for fused silica (Soileau et al., 1983) and alkali halide crystals (Garnov et al., 1993) in the pulse range of 4 ps to 31 ns.

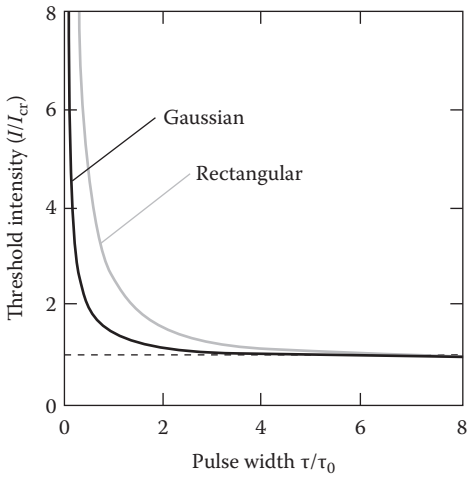

FIGURE 3.5 Normalized threshold intensity versus pulse duration normalized to absorber temperature relaxation time. (Reprinted figure with permission from Koldunov, M.F., Manenkov, A.A., and Pokotilo, I.L., Pulse-width and pulse-shape dependencies of laser-induced damage threshold to transparent optical materials, in *Laser-Induced Damage in Optical Materials: 1995*, H.E. Bennett, A.H. Guenther, M.R. Kozlowski, B.E. Newnam, and M.J. Soileau, eds., Vol. 2714, pp. 718–730, SPIE, Bellingham, WA. Copyright 1996 by SPIE.)

3.2.4 Influence of the Thermal and Optical Properties of the Absorber and Host Material

3.2.4.1 Thermal Properties

The role of thermal conductivity in the context of damage-threshold calculation is different for the host material and absorber (Walker et al., 1981; Lange et al., 1984). Reduced host thermal conductivity leads to slower heat removal from the heated absorber, which, in turn, leads to lower thresholds. In the case considered earlier of homogeneous heat deposition in the absorber, substituting $D = 3K_h/4\rho_a C_a$ into Equation 3.7 gives

$$F_0 = \frac{6.2\,T_c\sqrt{K_h}}{\gamma}\sqrt{3\rho_a C_a \tau}. \tag{3.13}$$

Here the threshold fluence varies as a square root of the host thermal conductivity. For obvious reasons, there is no dependence on absorber conductivity since the temperature is assumed homogeneous inside the absorber (no diffusion). Calculations (Fuka et al., 1990) using an exact solution of Equations 3.1 and 3.2 with the boundary conditions given by Equation 3.3, and accounting for inhomogeneous absorption inside the absorber, showed a relatively weak threshold dependence on host and absorber thermal conductivities. The effect is different for different absorber sizes, but, on average, damage threshold changes roughly by a factor of 2 per order of magnitude change in the host thermal conductivity. In contrast to host conductivity, thresholds increased on average for decreasing absorber conductivity. For a laser

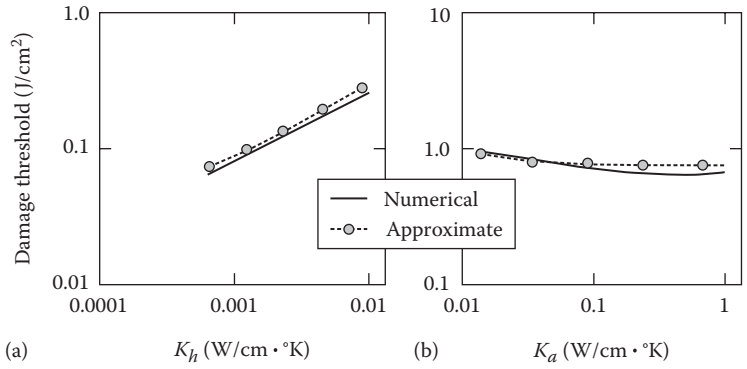

FIGURE 3.6 Damage threshold (a) for platinum impurity in glass as a function of host conductivity and (b) for ThO_2 impurity in a ThF_4 host as a function of absorber conductivity. (Reprinted figure with permission from Lange, M.R., McIver, J.K., Guenther, A.H., and Walker, T.W., Pulsed laser induced damage of an optical material with a spherical inclusion: Influence of the thermal properties of the materials, in *Laser Induced Damage in Optical Materials: 1982*, Nat. Bur. Stand. U.S. Special Publication, Vol. 669, pp. 380–386, U.S. Government Printing Office, Washington, DC. Copyright 1982 by SPIE.)

pulse length of $\tau \gg a^2/D_a$, an exact solution for the threshold F_0 given by Equation 3.4 can be simplified to (Lange et al., 1982, 1984)

$$F_0 = \frac{16T_c}{\pi}\sqrt{\rho_h C_h K_h \tau}\left[1+\frac{\pi\rho_a C_a}{120\rho_h C_h}\left(\frac{15\rho_h C_h}{\rho_a C_a}-10-\frac{K_h}{K_a}\right)\right]^{-1}. \tag{3.14}$$

Figure 3.6 shows the damage threshold for platinum impurity in glass as a function of host conductivity and ThO_2 impurity in ThF_4 as a function of impurity conductivity (Lange et al., 1982) calculated using exact numerical (Equation 3.4) and approximate (Equation 3.14) solutions. One finds a weak threshold dependence on absorber conductivity. Finite element analysis calculations (Papernov and Schmid, 1997) of the temperature fields around Hf metal and HfO_2 cylindrical nanoabsorbers (radius 5–20 nm, height 11–27 nm) also showed small changes in peak temperatures with conductivity variation.

3.2.4.2 Optical Properties

Optical properties of the absorber and host materials in the context of a thermal diffusion model affect damage thresholds through the heat source term A in Equation 3.1:

$$A = \frac{I\sigma}{V},$$

where $V = 4\pi a^3/3$ is the absorber volume. The key parameter to be calculated here is an absorption cross section σ_{abs}, which has the following general expression:

$$\sigma_{abs} = \sigma_{ext} - \sigma_{sca}, \tag{3.15}$$

where σ_{ext} and σ_{sca} are extinction and scattering cross sections, respectively. According to Mie's theory (we will use further Kerker's [1969] notation), σ_{ext} and σ_{sca} are defined as follows:

$$\sigma_{ext} = \frac{\lambda^2}{2\pi}\sum_{n=1}^{\infty}(2n+1)\left[\mathrm{Re}(a_n + b_n)\right],$$
$$\sigma_{sca} = \frac{\lambda^2}{2\pi}\sum_{n=1}^{\infty}(2n+1)\left(|a_n^2| + |b_n^2|\right), \tag{3.16}$$

where a_n and b_n are scattering coefficients that describe different electrical and magnetic multipole (dipole, quadrupole, etc.) contributions to light-wave scattering. These coefficients are expressed through combinations of the Riccati–Bessel functions and the Hankel functions of size parameters:

$$\alpha = \frac{2\pi a}{\lambda} \quad \text{and} \quad \beta = \frac{2\pi a m}{\lambda}, \tag{3.17}$$

where

λ is the wavelength in a medium

m is the relative complex refractive index, $m = m_1/m_2$, and indices 1 and 2 denote absorber and host, respectively

The refractive index of homogeneous dielectric host m_2 is real, $m_2 = n_2$, and absorber index m_1, in a general case, is complex, $m_1 = n_1(1 - ik)$.

The absorption cross section, σ_{abs}, as defined earlier (Equations 3.15 and 3.16), requires a rather complex numerical calculation. The calculation can be significantly simplified if size parameters α and β are small:

$$\alpha \ll 1 \quad \text{and} \quad |\beta| \ll 1. \tag{3.18}$$

It should be noted here that laser-quality glass and crystalline materials (fused silica, laser amplifier glass, KDP, DKDP crystals, etc.) have practically no visible defects in the bulk as observed using dark-field microscopy with white-light illumination (~550 nm center wavelength or ~370 nm in the medium with $n = 1.5$). Such observation suggests that absorbers in these materials are smaller than ~100 nm ($a < 50$ nm). It has also been shown (Feit and Rubenchik, 2004a) that these absorbers are not metal-type, strong absorbers. This bolsters the validity of small-size approximation given by Equation 3.18. In this case, extinction is dominated by absorption and σ_{abs} can be expressed (Kerker, 1969) using only the leading term (dipole term) of expansions for σ_{ext} (Equation 3.16):

$$\sigma_{abs} = -4\pi a^2 \alpha \mathrm{Im}\left(\frac{m^2 - 1}{m^2 + 2}\right). \tag{3.19}$$

Introducing ε_1 as an absorber dielectric function and using substitutions,

$$m = \frac{m_1}{m_2}, \quad m_2 = n_2, \quad m_1^2 = \varepsilon_1, \quad \varepsilon_1 = \varepsilon_1' + i\varepsilon_1'', \quad \alpha = \frac{2\pi a}{\lambda}, \quad \lambda = \frac{\lambda_0}{n_2},$$

Equation 3.19 takes the following form:

$$\sigma_{abs} = -\frac{24\pi^2 a^3 n_2}{\lambda_0} \mathrm{Im}\left(\frac{\varepsilon_1' + i\varepsilon_1'' - n_2^2}{\varepsilon_1' + i\varepsilon_1'' + 2n_2^2}\right). \tag{3.20}$$

Calculation of the imaginary part of the term in brackets gives

$$\sigma_{abs} = \frac{24\pi^2 a^3}{\lambda_0} \frac{\varepsilon_1'' n_2^3}{\left(\varepsilon_1' + 2n_2^2\right)^2 + \varepsilon_1''^2}. \tag{3.21}$$

One can see that the absorption cross section in the first approximation is proportional to a^3, or the volume of the absorber, and can be calculated for known dielectric functions. It also shows that absorption is more effective for shorter wavelengths and for the host medium with higher refractive index n_2. Equation 3.21 can also be used for very small, strong metal-type absorbers (Kreibig and Vollmer, 1995) like gold particles with a size less than ~20 nm. For larger particles, the scattering contribution (~a^6) to σ_{ext} becomes large enough and $\sigma_{abs} \cong \sigma_{ext}$ is not valid.

For small dielectric absorbers, an alternative approximate expression for σ_{abs} can be used (Walker et al., 1981; Kerker, 1969) if indices $n = n_1/n_2$ and k are in the range of $1 < n \leq 1.5$ and $0 < nk \leq 0.25$:

$$\sigma_{abs} = \pi a^2 \left[1 + \frac{\exp\left(-8\pi n_1 k \frac{a}{\lambda}\right)}{8\pi n_1 k \frac{a}{\lambda}} + \frac{\exp\left(-8\pi n_1 k \frac{a}{\lambda}\right) - 1}{\left(8\pi n_1 k \frac{a}{\lambda}\right)^2}\right]. \tag{3.22}$$

Figure 3.7 shows an example of exact calculations of absorptivity for a wide range of size parameters and absorption indices. A strong dependence on size is apparent for high absorption indices and for a relatively small parameter $\alpha \leq 1$. For large parameters $\alpha > 10$, absorptivity approaches unity, which means that the absorption cross section is approaching a value for a geometrical cross section. The earlier presented calculations (Bonneau et al., 2001) for metallic absorbers in Figure 3.2 show a behavior similar to that shown in Figure 3.7 for the highest absorption indices, with clear maximum and very slow changes for absorbers with a diameter $2a > 1000$ nm. In the same work (Bonneau et al., 2001), it was demonstrated that calculated damage threshold versus size dependences for Al absorbers at 351 and 1053 nm wavelength (see Figure 3.8) strongly

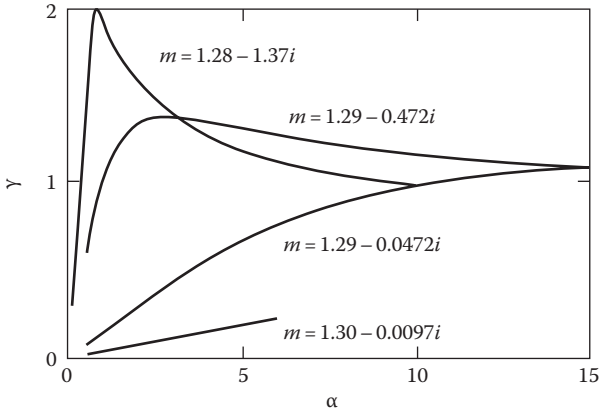

FIGURE 3.7 Absorptivity for various absorption indices as a function of parameter $\alpha = 2\pi a/\lambda$. (Reprinted from *The Scattering of Light and Other Electromagnetic Radiation*, Kerker, M. Copyright 1969, with permission from Elsevier.)

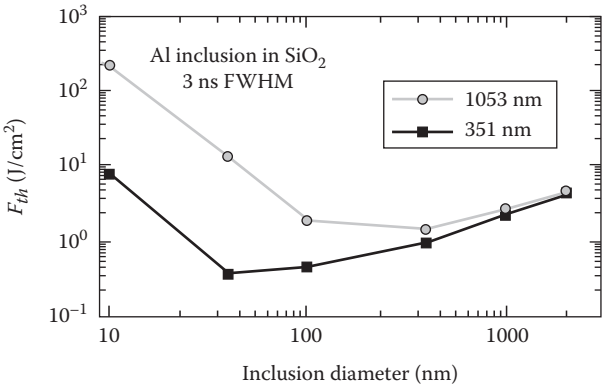

FIGURE 3.8 Damage threshold for Al absorber in SiO_2 and two laser wavelengths, 351 nm and 1053 nm, as a function of Al absorber size. (Reprinted figure with permission from Bonneau, F., Combis, P., Vierne, J., and Daval, G., Simulations of laser damage of SiO_2 induced by a spherical inclusion, *in Laser-Induced Damage in Optical Materials: 2000*, G.J. Exarhos, A.H. Guenther, M.R. Kozlowski, K.L. Lewis, and M.J. Soileau, eds., Vol. 4347, pp. 308–315, SPIE, Bellingham, WA. Copyright 2001 by SPIE.)

correlate with the behavior of absorptivity shown in Figure 3.2. Note the strong wavelength dependence (more than the order of magnitude difference) for small, ~10 nm absorbers, and vanishing wavelength dependence for large, >1000 nm absorbers.

3.2.5 Influence of Absorber Geometry and Orientation

It is of interest to compare the results from applying a thermal diffusion model to three standard absorber geometries of an absorber—plates, rods, and spheres. Such geometries correspond to one-, two-, and three-dimensional diffusion with a characteristic size parameter l equal to the half-thickness of the plate and the radius for rods and spheres.

Calculation of peak temperatures, assuming for simplicity the same material for absorber and host, and homogeneous energy deposition at a constant rate (constant intensity, flat-in-time laser pulse), yields the following results for plates (index 1), rods (index 2), and spheres (index 3) (Trenholme et al., 2006):

$$T_1 = \frac{\beta F}{C_V}\left[1-\left(1+\frac{2}{\nu}\right)erfc\left(\frac{1}{\sqrt{\nu}}\right)+\frac{2}{\sqrt{\pi\nu}}e^{-1/\nu}\right],$$

$$T_2 = \frac{\beta F}{C_V}\left[1-e^{-1/\nu}+\frac{E_1\left(1/\nu\right)}{\nu}\right], \tag{3.23}$$

$$T_3 = \frac{\beta F}{C_V}\left[1-\left(1-\frac{2}{\nu}\right)erfc\left(\frac{1}{\sqrt{\nu}}\right)-\frac{2}{\sqrt{\pi\nu}}e^{-1/\nu}\right],$$

where

- β is the absorption coefficient
- F is the laser fluence
- C_V is the heat capacity per unit volume
- E_1 is the exponential integral
- ν is the normalized time, given by the actual time divided by the diffusion time for a characteristic distance l:

$$\nu = \frac{4Dt}{l^2}.$$

The quantities inside the square brackets are the diffusion factors, and the term in front gives temperature rise in the absence of diffusion ($t \ll l^2/4D$).

The peak temperature is always reached at the end of the pulse and, *for times much longer than the diffusion time* $l^2/4D$, scales as $t^{1/2}$ for plates and $\ln(t)$ for rods. For spheres, the peak temperature asymptotically approaches a constant value equal to the no-diffusion value and heating applied over time period twice the diffusion time. This result shows that the plate- and rod-shaped absorbers are more effectively heated than the balls and, consequently, should fail at lower laser fluences.

In the case of plates and rods, an additional parameter to be accounted for is the orientation relative to the beam-propagation direction. The results of calculations given by Equation 3.23 are for the laser beam propagating normal to either the plate or the rod axis. For different orientations, the energy deposition rate is proportional to the cosine of the angle between the laser beam and vector normal to the plate surface, and proportional to the sine of the angle with the rod axis. In the case of random absorber orientations, this will reduce the number of absorbers failing at particular laser fluence, exceeding the threshold value.